Winter 2023

Biological Oscillator Synchronization with the Cellular Potts Model

Rose Una

Biological Oscillator Synchronization with the Cellular Potts Model

Rose Una

March 2023

Abstract

Similar to the way in which neurons synchronize their firing in the brain, individual cells of certain single-celled species can synchronize their internal molecular clocks to those of their neighboring cells. We develop an abstract Cellular Potts Model (CPM) to analyze this oscillator synchronization with two-dimensional cells on a square lattice. Model assumptions and constraints are motivated by behavior in single-celled species of slime mold (*Dictyostelium discoideum*) and slime bacteria (myxobacteria). In the CPM framework, cell-cell adhesion, which is influenced by variable clock updates per time step, and cell movement are governed by the so-called Hamiltonian energy function. The effects on oscillator synchronization of the spatial attraction parameter and the neighboring clock coordination parameter are explored in this project. We find four distinct steady phase states which cells' clocks converge to as a result of different parameter value combinations: global synchronization, local synchronization, incoherence, and anti-synchronization. Results include phase diagram, synchronization, and cell movement analysis. The findings of this project are applicable to pattern formation in cell cultures.

1 Introduction

Pattern formation in biological cell clusters is the result communication and/or complex interactions between the involved cells [5, 7]. Slime bacteria (myxobacteria) and slime mold (*Dictyostelium discoideum*) are two species of single-celled organisms that display this type of behavior amongst colonies of their own type. Under certain circumstances, these species form aggregates that go through a sequence of behavioral steps. A wave-like ripple effect can start traveling through the aggregate of cells. Then, fruiting bodies form such that the cell aggregates grow into larger three-dimensional forms [7]. We seek to understand the mechanisms underpinning the aggregation of biological cells through the development of an abstract computational model exploring cell movement and the processes causing such aggregation behavior.

This form of cellular aggregation is believe to be motivated by synchronization of molecular clocks housed within each cell of the cluster. The oscillation of these molecular clocks can be categorized by the Kuramoto model of oscillatory mechanisms and synchronization in individual bodies [4, 3]. We apply the point-based synchronization and movement oscillator Kuramoto-based model of O'Keeffe et al. [4] to a Cellular Potts Model (CPM) [2], which considers the functionality of biological cells. Therefore, our model combines the point-based oscillators with biological cells to capture movement, adhesion interactions, and oscillator synchronization in two-dimensional cells. The CPM, also known as the Glazier-Graner-Hogeweg model, is an computational agent-based model that simulates biological cell behavior through optimization of features such as the shape, location, and adhesion of cells that each take up some number of adjacent lattice sites on some form of a lattice grid. The CPM uses the Hamiltonian energy function to minimize each cell's energy at each time step.

Synchronization behavior of the cell oscillators, or clocks, is similar to the neurons firing synchronously or fireflies flashing synchronously. To capture the synchronization of the included cells' molecular clocks, we apply the Kuramoto-based oscillatory mechanisms [3] such that each cell has an internal oscillating clock and the optimization Hamiltonian energy function in the CPM includes a term that adjusts cell-cell adhesion dependent on neighboring cell clock times, also called phases. Our model includes two primary equations, the Hamiltonian and a recursive cell-clock calculator. We choose control parameters [8] that retain cellular integrity. We identify two manipulative parameters

that influence cell clock synchronization [4]. One manipulated parameter is responsible for the spatial attraction between cells through influencing their adhesion strength to each other on the basis of clock phase value differences. The second manipulated parameter is responsible for how cells orient themselves with respect to their neighboring cells.

We model the behavior within a predetermined population of cells and between their individual cell clocks. We seek to identify and understand the different steady phase states cells sort themselves into based on their clock phase synchronization behavior and dependent upon different manipulated parameter value combinations. We find four distinct phase states that the cells in a given simulation run can converge to depending on the predetermined manipulated parameter value combination. When cells seek to synchronize with their neighbors and are attracted to other cells with a like phase, as preset by manipulated parameter values, then the there is global synchronization. Surprisingly, we find faster global synchronization when cells seek to synchronize with their neighbors but are attracted to other cells in an opposite phase than when they are attracted to other cells with in like phases.

We define the four distinct phase states qualitatively with a phase diagram and quantitatively with order parameters. These phases states include global synchronization, local synchronization, incoherence, and anti-synchronization. Effects of the different phase states on cell movement and synchronization rate is explored.

2 Methods

We develop an abstract CPM [2] to investigate internal oscillatory synchronization and is motivated by the behavior of slime bacteria (myxobacteria) and slime mold (*Dictyostelium discoideum*) species. Each cell is modeled as a group of adjacent square sites in a square lattice. Each cell has an internal oscillator. In our model, the number of cells on the lattice is predetermined as N. Motion of and interaction between cells are based on an energy minimization scheme involving a Hamiltonian energy function. In this discrete model, in the internal clock of each cell continually moves forward slowly by default. However, by allowing adhesion between cells to be affected by clock phases of neighboring cells, there is variability to clock phases. They can change depending on minimization conditions in the Hamiltonian energy function and in the actual clock phase update function. Additional constraint terms are incorporated into the Hamiltonian as seen fit. The governing Hamiltonian is

$$\mathcal{H} = \sum_{\text{neighboring sites } \mathbf{i},\mathbf{j}} (1 - \delta_{\sigma(\mathbf{i}),\sigma(\mathbf{j})}) f(\sigma(\mathbf{i}), \sigma(\mathbf{j})) + \lambda \sum_{\text{cell } s} (\text{Area}(s) - A_{\text{target}})^2. \tag{1}$$

Here $\sigma(\mathbf{i})$ denotes the index of the cell occupying the lattice site $\mathbf{i}$. The first term of the Hamiltonian describes cell-cell adhesion between adjacent cells. δ_{ij} is the Kronecker function: $\delta(i,j) = 1$ if $i = j$, and $\delta(i,j) = 0$ if $i \neq j$. The Kronecker function allows the Hamiltonian to not consider the same lattice site twice. The cell-cell adhesion term $f(\sigma_1, \sigma_2)$ is given by

$$f(\sigma_1, \sigma_2) = \begin{cases} J_0(1 - J\cos(\theta_{\sigma_1} - \theta_{\sigma_2})) & \text{if } \sigma_1 \neq 0 \text{ and } \sigma_2 \neq 0 \\ J_0 & \text{if } \sigma_1 = 0 \text{ or } \sigma_2 = 0 \end{cases} \tag{2}$$

where σ_1 and σ_2 are neighboring cells. Index $\sigma = 0$ represents extracellular matrix (ECM), which has contact energy of J_0. Equation (2) computes the adhesion energy between neighboring cells through iterative computations and takes into consideration if the neighboring cells are merely ECM. Our choice of J_0 influences whether cells prefer to adhere to each other, regardless of phase, or prefer to be completely surrounded by ECM.

The second term of the Hamiltonian is a cell area constraint term. We use A_{target} and λ based on previous studies [8]. Time evolution is modeled via Monte Carlos Steps (MCS). Thereby, each cell's energy is calculated at each MCS with all its actions (movements, growth, molecular clock behavior) seeking to minimize its energy footprint via the Hamiltonian. Cell behavior established by the Hamiltonian considers a cell and its neighbors. Neighboring cells of an individual cell are defined as the cells and/or medium that shared common surface area with the individual. Therefore, cells must be in contact to influence each other's movements and, discussed later, their clock phases. We use general neighbor order of two [4, 8].

Lattice sites are denoted by bold variables $\mathbf{i} = (i_1, i_2)$. Each lattice site $\mathbf{i}$ is occupied by one of N cells or ECM. Hence, $\sigma(\mathbf{i}) = 0$ if the medium occupies $\mathbf{i}$ and $\sigma(\mathbf{i}) =$ *"cell index"* otherwise. Cell

movement is determined in spin flips, which are probabilistic determiners of cell movement based on whether or not a movement would minimize the cell's energy through the Hamiltonian function. After the energy for a step is calculated for each cell in a MCS via the Hamiltonian, a spin flip attempt occurs at each lattice site and inherently for each cell to determine whether the cell will make a calculated move to an adjacent lattice site, change shape, change size, etc. Spin flips are calculated by chance to incorporate $\Delta\mathcal{H} \leq 0$. The probability of a spin flip is given by

$$P_{\text{spin flip}} = \begin{cases} 1 & \text{if} \quad \Delta\mathcal{H} \leq 0 \\ e^{\frac{\Delta\mathcal{H}}{T}} & \text{if} \quad \Delta\mathcal{H} > 0 \end{cases} \tag{3}$$

where T is the temperature of the system and $\Delta\mathcal{H}$ is the change in energy that would result from a cell making the calculated change (acting on the spin flip). Higher temperatures make it more likely for spin flips to occur but also make it more likely for cells to fragment, dissolving into each other. By equation (3), a spin flip is taken if $\Delta\mathcal{H} \leq 0$ such that $P_{\text{spin flip}} = 1$ where a cell obtains a new lattice site and grows or moves one of its pixels to a new lattice site. A spin flip is attempted at each lattice site for each MCS. Spin flips are taken/successful with probability $P_{\text{spin flip}}$.

Our chosen parameter values are motivated by those of others' model development [5, 8]. See the below table for the control parameters used in our CPM. The only added constraint to the Hamiltonian function (1) beyond adhesion and cell movement is target area. The constant clock speed parameter ω is chosen on the premise of what is reasonable for tracking the oscillation of the cells' molecular clocks.

Parameter	**Value**	**Description**
Lattice dimensions	126x126	*Cartesian (square) lattice size
T	20	Temperature
θ_0	$U([0, 2\pi])$	*Uniform distribution of initial clock phases
A_{Target}	25	Target cell area
λ	25	Cell area stability term
ω	0.001	*Clock speed
J_{MM}	0	Medium-medium contact local product adhesion energy
$J_{CM} = J_0$	16	Medium-cell contact local product adhesion energy
$f(\sigma_1, \sigma_2)$	See (2)	Cell-cell contact local product adhesion energy
	2	Neighbor order
N	445	*Cell count
	0.7	*Confluency

Table 1: Parameter Table. Control parameters from Zhang et al [8]. *Parameters we chose.

Now that we have addressed the foundation of the CPM, we look to the oscillatory processes housed in each cell of the model that seek to simulate molecular clocks in real cells. Each cell $s = 1, \ldots, N$ in the model has an internal oscillating clock. This clock reads phases, similar to times, as θ_s, which is a time-dependent scalar that updates each MCS via

$$\theta_s^{t+\Delta t} = \theta_s^t + \omega\Delta t \cdot (1 + K \cdot \frac{1}{\#\text{ neighbors of } s} \sum_{\text{neighbor } u \text{ of } s} \sin(\theta_u - \theta_s)) \tag{4}$$

As shown in (4), a cell's internal clock is influenced by the clocks of its neighbors. At the beginning of the simulation run, initial clock phase values are randomly assigned for all cells in a uniform distribution of $[0, 2\pi]$. Once the model simulation starts running, each cell's clock phase changes according to (4) and with speed ω. Cells' clocks do not tick forward at a linear rate. The clock phases of a cell's neighbors influences the clock phase of the given cell. The correlation between a cell's clock phase and those of its neighbors is one of two primary interests in parameters. K, in (4), is the phase coupling strength between neighboring cells [4]. It controls how neighboring cells' clocks influence each other. For $K > 0$, neighboring cells seek to synchronize their clock phases. For $K < 0$, neighboring cells seek to anti-synchronize their clocks. To synchronize, neighboring cells have clock phases θ_i=θ_j in $[0, 2\pi]$. To anti-synchronize, neighboring cells have clock phases that off by pi such as $\theta_i = 0$ and $\theta_j = \pi$.

The second parameter of of interest is J found in (2), which is the spatial attraction parameter [4]. For $J > 0$, cells of like phases attract each other. For $J < 0$, cells of opposite phases attract each other. Therefore, J influences cell-cell adhesion, thus influencing the rate at which cells synchronize their internal clocks to those of neighboring cells.

Parameters K and J (see equations (4) and (2), respectively)) are of interest as they are potentially the most influential parameters in determining cell oscillator synchronization. K is responsible for the behavior of cells with respect to their neighbors. Therefore, K affects the synchronization patterns of the cells. J, in 2, determines how clock phase differences affect cell-cell adhesion, ultimately deciding if similar clock phases of neighboring cells lead to mutual attraction or repulsion [4]. We hypothesize that for $J > 0, K > 0$, cells will aggregate into clusters of synchronized clocks. Therefore, our guiding research question follows: how is the "regularity" of the pattern of cell aggregates influenced by the strength of the synchronization of cell phases?

To implement the Cellular Potts Model, we use the open-source software CompuCell3D [6]. CompuCell3D uses Python, C++, and XML languages to implement ad develop biological cell models. The implemented model is based on that of which is described in Alber et al[1].

3 Results

We test combinations of J, K parameter values to understand their role in cell aggregation and synchronization. There are four long-term behavioral steady phase states of cell clock distribution based on model predetermined J, K parameter values. The phase states are global synchronization, local synchronization, incoherence, and anti-synchronization. See Figure 1 for visual distinction between the phase states. Our results are to be similar to those by O'Keeffe et al [4] with variation by cells with areal significance.

Variations in J and K express different priorities of the cells. Parameter J affects the adhesion strength between cells. Parameter K influences a cell's clock phase variability with respect to synchronization with neighbors. See the table below describing the effects of different J and K values since the sign of the manipulated parameter effects cell behavior.

Parameter	**Sign**	**Effect of a cell's phase**
J	$J > 0$	"Phases attracts like phases"
	$J < 0$	"Opposite phases attract"
K	$K > 0$	"Neighbors seek to synchronize"
	$K < 0$	"Neighbors seek to anti-synchronize"

Table 2: Manipulated Parameter Table.

3.1 Phase Diagram

We identify the role of different J, K parameter combinations in equations (2) and (4) by comparing long-term behavior of cell clocks with varying J and K. The corresponding phase diagram is the representation of a parameter scan for J and K with consistent initial conditions for each run. Each of the forty-nine squares in Figure 1 represent an individual simulation run with a different $J - K$ value combination but each with the same initial cell position and initial clock phase distribution.

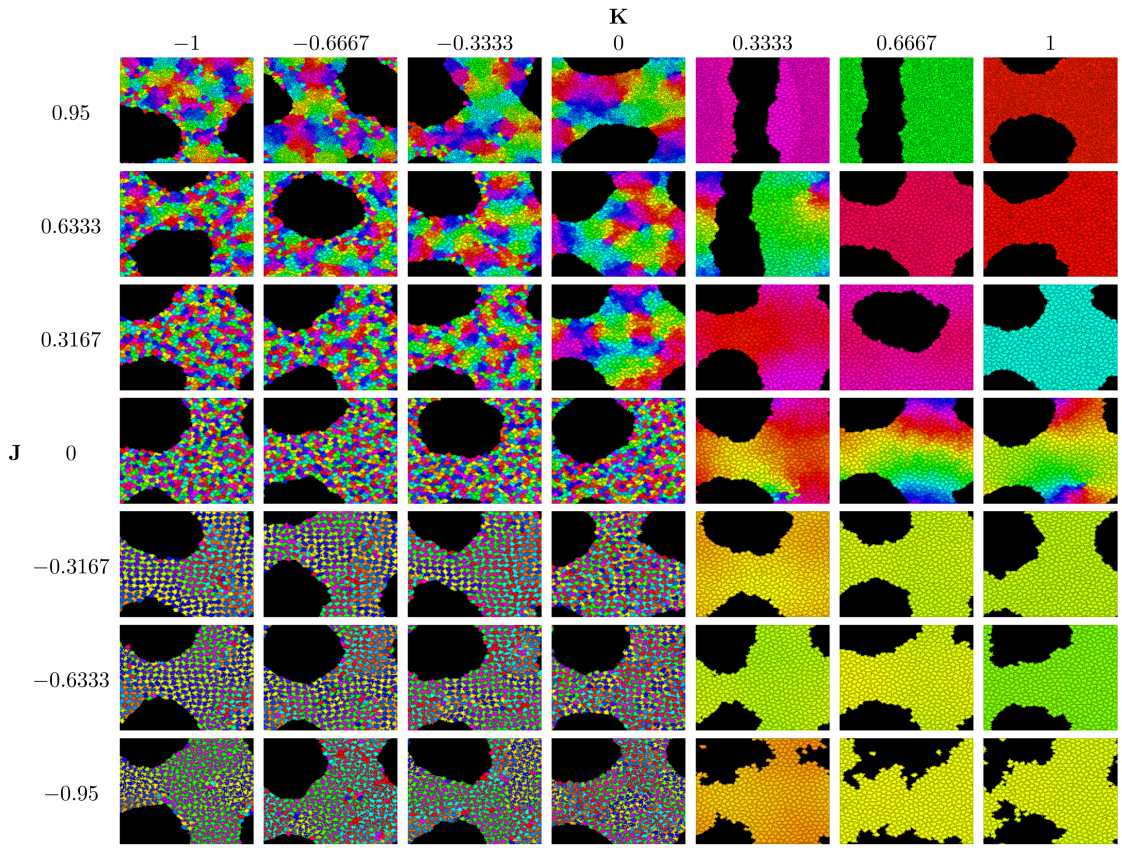

Figure 1: Phase diagram. Cells are colored according to their clock phase. For the possible ranges of J and K, the four distinct phase states are present: global synchronization ($K > 0$), local synchronization ($J > 0, K \leq 0$), incoherence ($J \geq 0, K < 0$), and anti-synchronization ($J < 0, K \leq 0$). Simulation runs were each of $N = 445$ cells for 250,000 MCS and the same initial conditions.

Since the cell clocks are ticking forward at rate ω beyond consideration of neighboring cell clocks, we take each cell clock modulo 2π to retain oscillatory phase values. Without taking modulo 2π of each cell clock, we consider the time each cell clock reads as a value that can trail off toward $+\infty$ or $-\infty$. We want to retain a mechanical clock pattern for keeping time such that the time-keeping restarts at 0 over as soon a cell's phase reads $\theta = 2\pi$.

For manipulated parameter values, we chose $J = [-0.95, -0.6333, -0.3167, 0, 0.3167, 0.6333, 0.95]$ and $K = [-1, -0.6667, -0.3333, 0, 0.3333, 0.6667, 1]$. As for having seven terms for both J and K, we needed few enough value options for computational efficiency but enough values for clear resolution on cell sorting behavior. We expect that choosing smaller increments within the J and K sets, we would get the same results at a finer resolution. The phase diagram shows all the cells in roughly the same global-scale organization because EMC energy $J_0 = 16$. Cells prefer to adhere to each other as compared to adhering to the EMC since choice of J_0 suggests cell-cell contact is less costly to Hamiltonian energy than is cell-ECM contact.

The following are qualitative descriptions of each of the four phase state as well as quantitative distinctions between them. We use order parameters to quantitatively distinguish between the observed phase states. An order parameter is an expression equal to zero in one phase of the system and non-zero in another phase, capturing the transition from one phase to another.

3.1.1 Global Synchronization

When all cells in a simulation run are in the same phase, we say the cells are in the phase state of global synchronized. Neighboring cells synchronize their clocks such that the expressed phase of each is identical. For $K > 0$, we find global synchronization. See Figure 1 where all the cells are the same color. Global synchronization is expected for $K > 0$ because cells seek to synchronize with their

neighbors. For both $J > 0$ ("like attracts like") and $J < 0$ ("opposites attract"), neighboring cells synchronize to the extent of global synchronization through agency of $K > 0$.

For $K > 0$, where we find global synchronization in 1, cells globally synchronize to different phase values as seen as different colors in the phase diagram. Even though different runs result in different phases (colors), we see primarily global synchronization for $K > 0$ because all the cells in any simulation run are the same color. We ran each simulation of the phase diagram with the same initial conditions (initial position, cell-clock uniform distribution, and cell clock assignment). Therefore, difference in end-behavior phase is the result of the inherent stochasticity of the model through spin-flip probability. The varying end-behavior phases are a matter of cells synchronizing to what we see as the majority of cells. It would take further investigation to definitively if there is reasoning for differing end-behavior phase value across globally-synchronized cells beyond the stochasticity of the CPM. However, our interests lie in the sameness of cell clock at the end of each run, creating global synchronization for specific K.

By our definition of global synchronization, some simulation runs in Figure 1 for $K > 0$ are not completely globally synchronized. In these instances, we presume that all the runs for $K > 0$ would reach complete global synchronization given enough MCS time steps, longer than the shown 250,000 MCS. Reasons for needing more time include the effects of the variation in magnitude of K and J as well as the inherent randomness involved with a particular model run.

We use the Kuramoto order parameter to gauge the degree of synchronization within the cells of a run at a given time step. This Kuramoto order parameter is based on the Kuramoto Model as used in by O'Keefe et al [4]. The global Kuramoto order parameter [3] captures the transition from global synchronization to any other phase states for the phase diagram in Figure 1. This order parameter is given by

$$r_{\text{global}} = \left| \frac{1}{N} \sum_{j}^{N} e^{i\theta_j} \right| \tag{5}$$

where N is the total number of cells in the simulation run and the resulting r is such that $r \in [0, 1]$. The r_{global} quantifies how synchronized all cells' clocks are within a single simulation at a specified MCS. If $r = 1$, all the cells' clocks are synchronized. If $r = 0$, all the cells' clocks are entirely unsychronized or anti-synchronized, meaning that all of their values are spread around the time clock evenly such that all values cancel each other out or there are synchronized groups of opposite phases that cancel each other out.

We calculate r_{global} for the same simulations of the phase diagram in Figure 1.

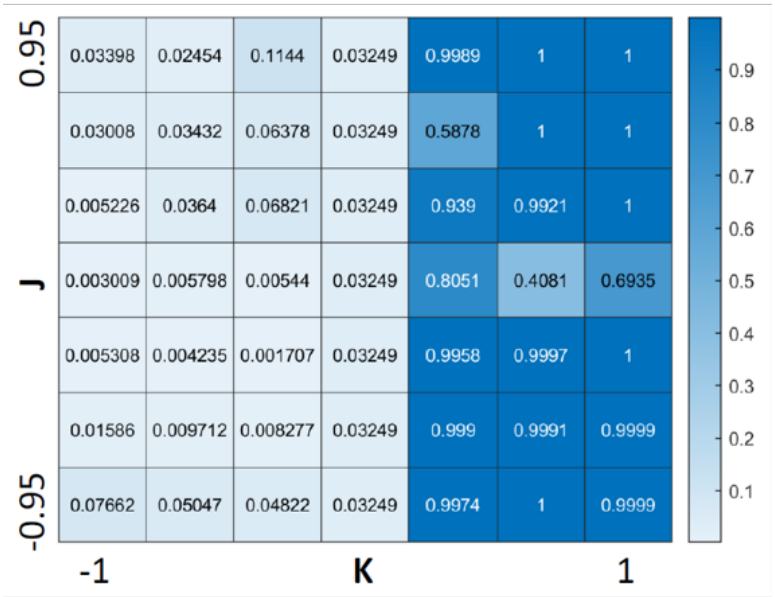

Figure 2: Global synchronization order parameter heat map. Global synchronization is characterized by $r = 1$. Synchronization was taken at the $250,000^{\text{th}}$ MCS.

There is a clear distinction between globally synchronized combinations of J, K and the other phase states. This distinction follows the phase diagram such that global synchronization occurs for $K > 0$ and all J.

3.1.2 Local Synchronization

Local synchronization is characterized by neighborhoods of cells synchronizing to the same phase without synchronization between neighborhoods. Synchronization between neighborhoods would lead to global synchronization. In Figure 1, the steady state behavior of local synchronization is visualized by patches of cells within an individual simulation run that are the same color (phase). We find local synchronization somewhere within the $J > 0, K < 0$ quadrant. Because cells seek cells in a like phase but want to anti-synchronize with their neighbors, we have only local synchronization instead of global synchronization. We see a transition somewhere in the $J > 0, K < 0$ quadrant from local synchronization to incoherence. Roughly, this transition happens at the $K = -J$ line. Further work into this region analytically or computationally could find this division between local synchronization and incoherence phase states more easily.

The local Kuramoto order parameter [3] describes the phase state of local synchronization. The only difference to the global synchronization r_{global} in Figure 5 is that synchronicity is measured over neighborhoods of cells of order 2 instead of measured over the whole population of cells. Neighborhood order is chosen to stay consistent with control parameters [8] used to run the model. Local synchronization is calculated through

$$r_{\text{local}} = \left| \frac{1}{s} \sum_{j}^{s} e^{i\theta_j} \right| \tag{6}$$

where s is the number of neighbors cell j has and r_{local} is calculated for every cell's neighborhood. Therefore, each cell has a local Kuramoto at any given MCS. For our calculations, the r_{local} of each cell is averaged over all cells in the simulation. Undoubtedly, there is local synchronization where there is global synchronization because neighborhoods of cells must be synchronized, too.

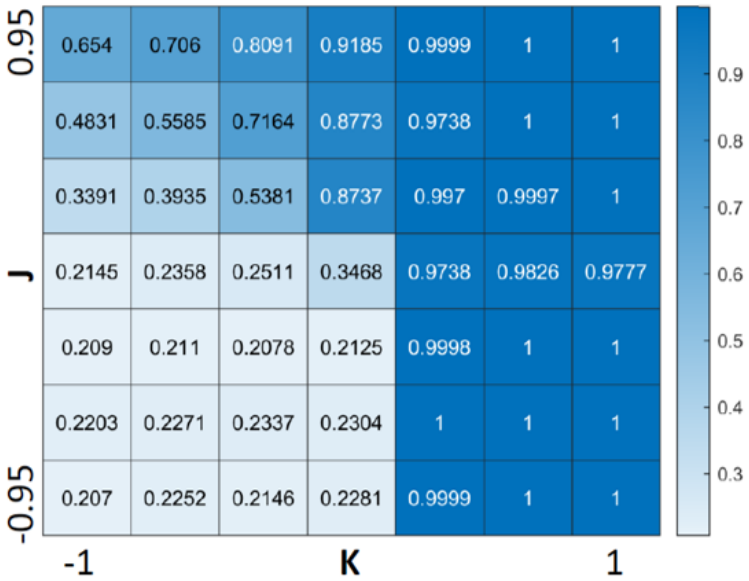

Figure 3: Local synchronization order parameter heat map. Complete local synchronization of neighborhoods to the second order is characterized by $r = 1$. Synchronization was taken at the $250,000^{\text{th}}$ MCS and is the average r_{local} of all individual cells' r_{local}.

In the above heat map, we find local synchronization for $K > 0$ and roughly $J > 0, K \leq 0$. This heat map clearly shows that somewhere in the second quadrant where $J > 0, K \leq 0$ there is a transition out of local synchronization into incoherence as J decreases toward 0.

3.1.3 Anti-Synchronization

The anti-synchronized phase state is characterized by cells of opposite phases attracting each other ($J < 0$). Furthermore, cells seek to anti-synchronize with their neighbors ($K < 0$). The resulting behavior is a chess board-style distribution of cell phases where cells minimize their energy by surrounding themselves with cells of the opposite phase.

The chess board order parameter describes the anti-synchronization phase state. This order parameter is named after the contrasting cell phases that are located next to each other, creating a chess board pattern. To quantitatively characterize anti-synchronization, we calculate the extent to which neighboring cells' clock phases are in opposite phase. We need some tolerance since neighboring cells will not be completely in opposite phase all the time. We chose a tolerance of 6.25% from total anti-synchronization between neighboring cells. To have neighboring cells in opposite phase, cell A would have a clock phase of 0 while its neighbor cell B, whom which cell A shares common surface area, would have a clock phase of π. In determining the locations of anti-synchronization in the $J-K$ plane, we find the following figure.

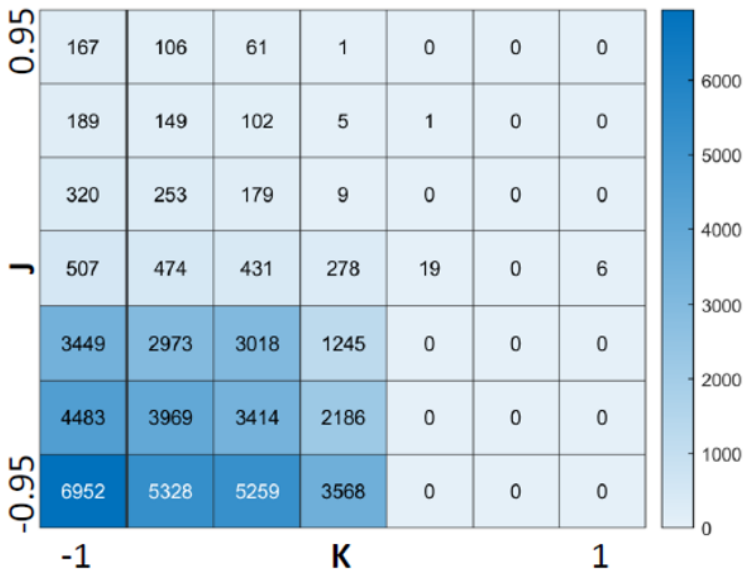

Figure 4: Chess board order parameter heat map. Anti-synchronization between neighboring cells is seen found only for $J < 0, K \leq 0$.

The chess board order parameter captures the specific combination of J and K that distinguishes the anti-synchronization phase state from the other phase states. $J < 0$ signifies that cells of opposite phase attract and $K \leq 0$ signifies that cells prioritize having neighbors of opposite phase.

3.1.4 Incoherence

The incoherent phase state is characterized by randomness in how cells organize themselves based on their clock phases. There does not seem to be a patterned organization to the cells. In Figure 1, this state is observed by cells of any phase neighboring cells of any other phase. We find this in the $J \geq 0, K < 0$ quadrant, just like the local synchronization phase. However, this state is seemingly below the $K = -J$ line and we do see that there is a transition from local synchronization to incoherence in the $J > 0, K < 0$ quadrant.

To characterize the incoherence phase state with order parameters, we can use the local Kuramoto order parameter in Figure 3 and the chess board order parameter in Figure 4. By overlaying these two heat maps, we would see that there is section within $J \geq 0, K > 0$ where the order parameter is zero or near zero in value. This "missing piece" is where the incoherence phase state exists, not included as locally synchronized nor anti-synchronized.

3.2 Synchronization and Movement

Cells' clocks synchronize such that after some time, their phases converge to a value a stay in that place for the rest of the simulation. The cells reach a steady state that can be categorized into one of the distinct phase states. To analyze the synchronization rates of simulations with different $J - K$ parameter value combinations, we analyze the Kuramoto r_{global} over so many MCS.

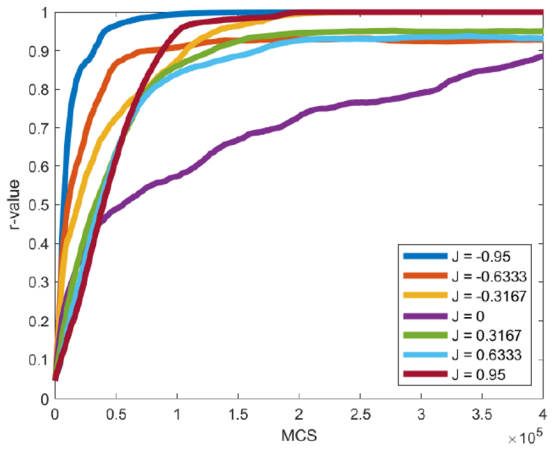

Figure 5: Global synchronization of cells over time. Synchronization was calculated using the Kuramoto equation (5). Each J-value plot has $K = 1$ and is the average of ten runs of the same J and K values, just different initial conditions.

The Kuramoto r value captures the global synchronization of all the included cells' clocks to determine if they are the same. If the cells' all have the same phase, meaning they are synchronized, we will find $r = 1$. If there is complete incoherence or anti-synchronization of the cells' clocks, we will find $r = 0$. Neighboring cells seek to synchronize but spatial attraction varies from opposites attracting ($J < 0$) to cells of like phases attracting ($J > 0$). We find synchronization of cells happen fastest in simulations where $J < 0$. Even though cells attract and adhere to those in opposite phase, they end up synchronizing faster than cells that seek to find cells in like phase as them.

The mean square displacement (MSD) of cells measures the distant a cell has traveled from its initial position to its new position after some amount of MCS averaged over all the cells in a single simulation run. We found that different J and K values affect the movement of the cells with respect of how far they travel.

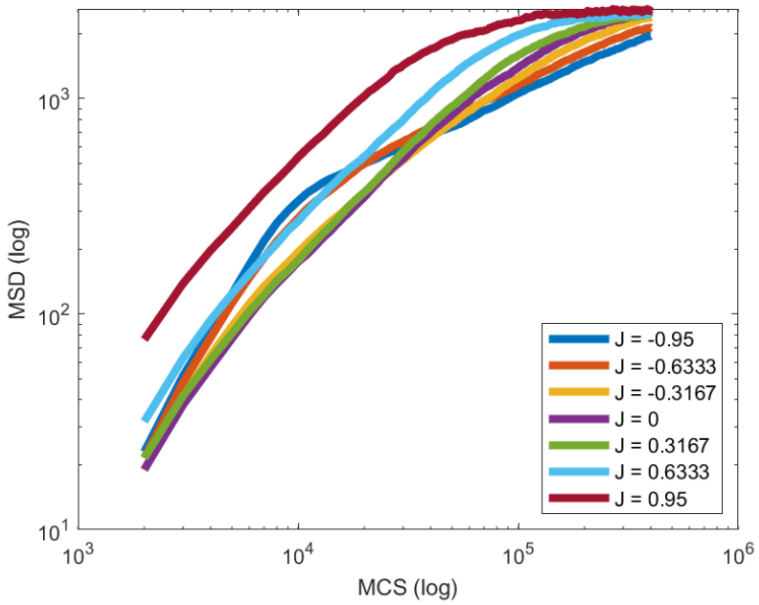

Figure 6: Mean Square Displacement. This is the log-log plot over seven J values, all with $K = 1$. Ten runs calculating the MSD to 400,000 MCS for each $J - K$ combination were averaged to create each of the given output functions.

Figure 6 shows that the larger the J-value, the more cells move and the smaller (and more negative) a run is, the cells move less. We primarily studied MSD for only $K = 1$ and different J values to conserve computational resources. Using $K = 1$, we remain in the global synchronization phase state as we analyze how the spatial attraction term J affects cell movement. We conclude that cells need to move most for $J > 0$ (like attracts like) because they seek out cells in like phase which requires lots of movement from the initial random positions and clock phase distributions. The opposite case holds true for $J < 0$ (opposites attract) such that cells of opposite phase attract, so individual cells do not need to travel as far to satisfy minimal adhesion energy related to J. Cells still synchronize because $K = 1$ but do so faster for $J < 0$, so they may not need to travel far to find others to synchronize to.

The data used to create 5 and 6 are the averages of ten runs simulations up to 400,000 MCS with different initial conditions (cell positions and uniform cell clock distribution).

4 Discussion

Through use of our CPM, we find four distinct phase states of which a simulation run can settle into depending on the predetermined J and K values. By changing whether or not cells seek to synchronize or anti-synchronize with their neighbors (K) and whether or not cells seek out others with the same or opposite phase (J), we find cells globally synchronize, only locally synchronize, globally anti-synchronize, or incoherently mix. Most fascinating is the parameter combination of $J < 0, K > 0$ where cells of opposite phases attract and neighboring cells attract. Even though cells of opposite phase attract ($J < 0$), global synchronization occurs faster that it does when cells of like phases attract ($J > 0$). We believe that in this situation of faster synchronization, cells seek out other cells in phases opposite of their own and in the process end up synchronizing. When cells of like phases attract ($J > 0$), they must move farther than when $J < 0$ to minimize their adhesive energy and find cells in like phase to them. Hence, synchronization happens slower for $J > 0$ than $J < 0$ when $K > 0$.

The CPM gets some criticism for the abstractedness of some of its parameters. The choice of control parameters [8] is motivated by creating as realistic cells as possible. Even so, we find some fragmenting of cells that blend with other cells for extreme values of J and K. Cell fragmentation is a demonstration of energy minimization because cells are not bothered by blending together if there is no energy cost to do so. We find fragmentation in cells of like phase for $J > 0$ and in cells of opposite phase for $J < 0$.

The CPM includes inherent randomness. This is beneficial from the naturalness of the model in which there is an unpredictability to the model or movement of the cells within the Monte Carlo component of the simulation. However, we must limit the randomness for the reproducibility of our scientific investigation. We can control the initial position of cells as well as the distribution of initial clock values by choosing the seed of each simulation and predetermined uniform distributions of cells with specified confluences.

Beyond further exploration of the effects of more K and J parameter-value combinations, making the model more realistic would make it more telling of what is happening in experimental work. This means developing structural cell characteristics such as cell polarity and chemotaxis [7]. With respect to further understanding phase synchronization, it would be worth exploring the rippling behavior of cell clocks we see in the interim period after initial cell movements and before complete end behavior. This behavior is most noticeable in the process of reaching local or global synchronization. Running simulations with confluences other than 70% would test the the critical cell population and spatial distribution necessary for aggregation and synchronization. A critique to this model is its lack of reliance on experimental data. By incorporating experimental data into control parameters and model constraints, we could take the next step towards connecting the phase states to physical cellular behavior.

References

[1] M. S. Alber, Y. Jiang, and M. A. Kiskowski, *Lattice gas cellular automation model for rippling and aggregation in myxobacteria*, Physica D: Nonlinear Phenomena, 191 (2004), pp. 343–358.

[2] n. Graner and n. Glazier, *Simulation of biological cell sorting using a two-dimensional extended Potts model*, Physical Review Letters, 69 (1992), pp. 2013–2016.

[3] Y. Kuramoto, *Chemical Oscillations, Waves, and Turbulence*, Courier Corporation, Jan. 2003. Google-Books-ID: 4ADt7smO5Q8C.

[4] K. P. O'Keeffe, H. Hong, and S. H. Strogatz, *Oscillators that sync and swarm*, Nature Communications, 8 (2017), p. 1504. Bandiera_abtest: a Cc_license_type: cc_by Cg_type: Nature Research Journals Number: 1 Primary_atype: Research Publisher: Nature Publishing Group Subject_term: Applied mathematics;Nonlinear phenomena;Phase transitions and critical phenomena Subject_term_id: applied-mathematics;nonlinear-phenomena;phase-transitions-and-critical-phenomena.

[5] C. H. Ramos, E. Rodríguez-Sánchez, J. A. A. Del Angel, A. V. Arzola, M. Benítez, A. E. Escalante, A. Franci, G. Volpe, and N. Rivera-Yoshida, *The environment topography alters the way to multicellularity in Myxococcus xanthus*, Science Advances, 7 (2021), p. eabh2278.

[6] M. H. Swat, G. L. Thomas, J. M. Belmonte, A. Shirinifard, D. Hmeljak, and J. A. Glazier, *Chapter 13 - multi-scale modeling of tissues using compucell3d*, in Computational Methods in Cell Biology, A. R. Asthagiri and A. P. Arkin, eds., vol. 110 of Methods in Cell Biology, Academic Press, 2012, pp. 325–366.

[7] S. Thutupalli, M. Sun, F. Bunyak, K. Palaniappan, and J. W. Shaevitz, *Directional reversals enable Myxococcus xanthus cells to produce collective one-dimensional streams during fruiting-body formation*, Journal of The Royal Society Interface, 12 (2015), p. 20150049. Publisher: Royal Society.

[8] Y. Zhang, G. L. Thomas, M. Swat, A. Shirinifard, and J. A. Glazier, *Computer simulations of cell sorting due to differential adhesion*, PloS one, 6 (2011), p. e24999.